Journal of The
Electrochemical Society

Is the Chemisorbed CO_2 in Ionic Liquid Electrolytes Active for Electrochemical Utilization? A Case Study on Carboxylate and Carbamate Speciation

To cite this article: Oguz Kagan Coskun *et al* 2025 *J. Electrochem. Soc.* **172** 066504

Journal of The Electrochemical Society, 2025 **172** 066504

Is the Chemisorbed CO_2 in Ionic Liquid Electrolytes Active for Electrochemical Utilization? A Case Study on Carboxylate and Carbamate Speciation

Oguz Kagan Coskun, Saudagar Dongare,* and Burcu E. Gurkan,z**

Department of Chemical and Biomolecular Engineering, Case Western Reserve University, Cleveland, Ohio 44106, United States of America

This study examines the activity of chemisorbed CO_2 species in the microenvironment formed by bifunctional ionic liquids (ILs) in the reactive capture and conversion (RCC) of CO_2 to CO on silver. Comparative electroanalytical measurements with imidazolium based ILs were performed to probe the impact of electrostatic interactions, anion and cation basicity, and hydrogen bonding on RCC. Particularly, ILs with 1-ethyl-3-methylimidazolium ($[EMIM]^+$) and 1-ethyl-2,3-dimethylimidazolium ($[EMMIM]^+$) cations and aprotic heterocyclic anions of 2-cyanopyrrolide ([2-CNpyr]) and 1,2,4-triazolide ([124-Triz]) were examined for RCC. It was found that anion–CO_2 carbamate complexes facilitate RCC at significantly lower overpotentials compared to cation–CO_2 carboxylate complexes. Additionally, $[EMIM]^+$ was found to better stabilize anion–CO_2 complexes at the interface than $[EMMIM]^+$. Furthermore, it was found that 2-CNpyrH that naturally forms during CO_2 absorption competes for electrode surface adsorption with the anion–CO_2 carbamate complex, thereby reducing the electrochemical activity of the anion–CO_2 complex. These results highlight the importance of IL structure in tuning the interfacial interactions and suggest that ILs with anion-dominated CO_2 chemisorption enhances CO_2 utilization in RCC applications.

 [DOI: 10.1149/1945-7111/addf83]

Manuscript submitted February 7, 2025; revised manuscript received May 19, 2025. Published June 11, 2025.

Supplementary material for this article is available online

The integration of CO_2 capture and electrochemical conversion has emerged as a promising strategy for mitigating carbon emissions while producing value-added products,[1] since it bypasses the costly intermediate CO_2 concentration stage.[2] Among the various electrolytes studied for reactive capture and conversion (RCC) of CO_2, ionic liquids (ILs) as an active electrolyte component received significant interest due to their ability to form unique interfacial structures[3] and absorb significant amount of CO_2.[4] Unfunctional ILs only physisorb CO_2; those with imidazolium cation may form carboxylate adducts with CO_2 when they are reduced to carbenes via proton liberation on the electrode surface. On the other hand, for imidazolium ILs with amine functionalized anions, the carboxylate formation in the bulk via carbene is a spontaneous reaction in the presence of CO_2.[5–7] Further, aprotic heterocyclic anions with amine moiety present nucleophilic sites for direct binding with CO_2, thus forming anion–CO_2 adducts, namely carbamate.[7–9] Thus, when the imidazolium cation is paired with such reactive anions, both carboxylate and carbamate species form upon CO_2 absorption with an equilibrium that is dependent upon the CO_2 partial pressure.[7] Therefore, in the presence of bifunctional ILs, where both ions are capable of speciation with CO_2, a dynamic interface including the additional hydrogen bonding complexes among these ion–CO_2 adducts contribute to the overall catalytic activity.[10,11] However, the reduction of the chemisorbed CO_2 in these adducts remain poorly understood to capitalize on the advantageous availability of CO_2 offered by bifunctional ILs for RCC.[12] To be specific, it has not been concluded with certainty if the chemisorbed CO_2 in the form of carboxylates and carbamates is utilized in RCC. In this study, the utilization of these specific species is examined in electrocatalytic conversion of CO_2 to CO on silver through a systematic and well-controlled speciation approach.

This study revisits CO_2-to-CO conversion on Ag in the presence of [EMIM][2-CNpyr] to determine whether carboxylate and carbamate species are directly utilized in RCC. Figure 1 illustrates the interfacial species present in the electrolyte after CO_2 exposure. Among these, $[EMIM]^+$ has been shown with the benchmark IL, $[EMIM][BF_4]$, to enhance CO_2 activation by reorienting parallel to the electrode surface at the interface, generating a local electric field that stabilizes intermediates.[13] The same behavior was also confirmed for [EMIM][2-CNpyr], where a similar orientation shift was detected.[11] Additionally, we demonstrated that the protonated anion 2-CNpyrH acts as a hydrogen bond donor, further facilitating CO_2RR and changing product selectivity.[11] While these findings clarify the role of $[EMIM]^+$ and 2-CNpyrH at the interface, it was not possible to distinguish the individual contributions of physisorbed and chemisorbed CO_2 species during RCC. To address this, we systematically probe their electrochemical behavior through voltametric experiments designed to isolate and analyze individual interfacial species. Specifically, the neat IL was first saturated with CO_2, then diluted in an organic solvent, and maintained under N_2 to eliminate physisorbed CO_2, thus selectively retaining the chemisorbed CO_2 species; this condition is referred as "pre-CO_2." These experiments were complemented by electrolysis product analysis to assess the conversion efficiency.

Materials and Methods

Materials.—1-ethyl-3-methylimidazolium chloride ([EMIM][Cl]) and 1-ethyl-3-methylimidazolium tetrafluoroborate ($[EMIM][BF_4]$) were purchased from Iolitec, while 1-ethyl-2,3-dimethylimidazolium chloride ([EMMIM][Cl]) was obtained from Thermo-Fisher. The anion precursors pyrrole-2-carbonitrile (2-CNpyrH, 99%) and 1,2,4-triazolide (97%) were sourced from Thermo-Fisher and MilliporeSigma, respectively. Anion exchange resin (IRN-87) was acquired from Purolite. Electrolyte salts tetraethylammonium tetrafluoroborate ($[EMIM][BF_4]$, 99%) and tetraethylammonium perchlorate (TEAP, >98%) were obtained from Sigma-Aldrich and BeanTown Chemical, respectively. Acetonitrile (99.9%) was also from Sigma-Aldrich, while methanol (99.8%, HPLC Grade) was supplied by Fisher Scientific. The gases CO_2 (99.995%) and N_2 (99.999%) were provided by Airgas. For nuclear magnetic resonance spectroscopy (NMR) characterization, deuterated dimethyl sulfoxide (DMSO-d6, 99.9% isotopic) was sourced from Thermo Scientific, and

*Electrochemical Society Student Member.
**Electrochemical Society Member.
zE-mail: beg23@case.edu

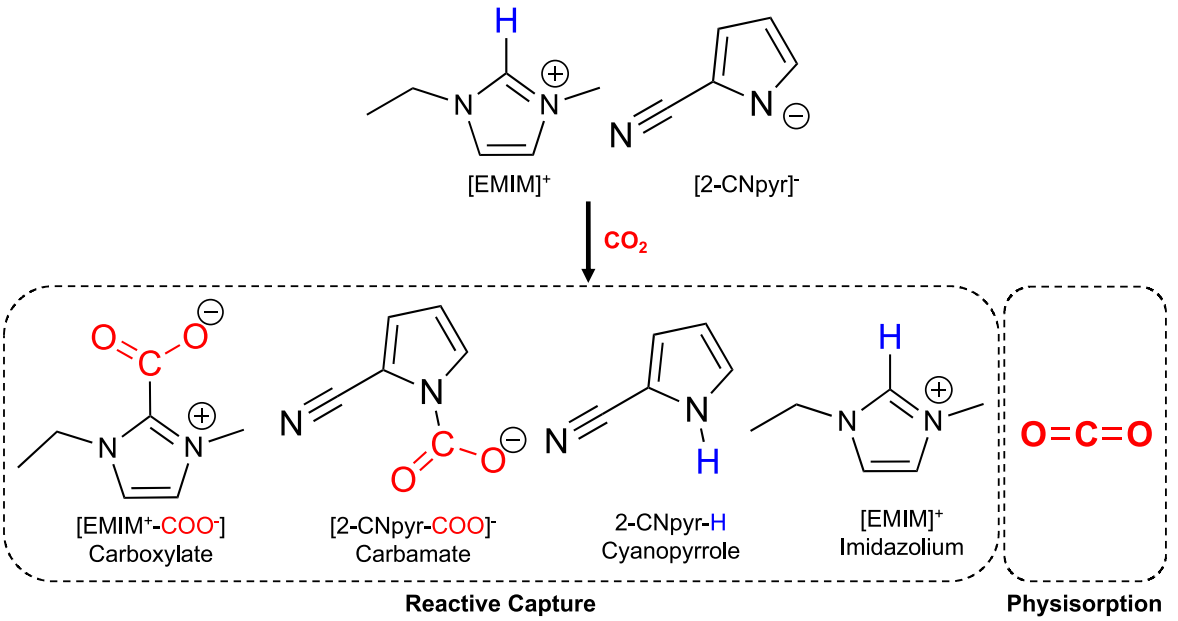

Figure 1. Structures of [EMIM][2-CNpyr] IL and CO_2 chemisorption products. In a CO_2-saturated IL electrolyte, both chemisorbed and physisorbed CO_2 species are present.

chromium (III) acetylacetonate (99%) was purchased from Sigma-Aldrich. NMR tubes were obtained from Bruker. All chemicals were used as received without further purification unless otherwise noted.

Reactive IL synthesis.—The synthesis of ILs followed a two-step anion exchange process, as previously reported for [EMIM][2-CNpyr][14] and also applied here for [EMIM][124-Triz]. In this method, the ILs were synthesized starting from halide salts of the cation precursor, converting them into their hydroxide form, followed by a reaction with the respective anion precursor.

For [EMIM][2-CNpyr] and [EMIM][124-Triz], the chloride salt of the cation ([EMIM][Cl], 98%, IoliTec) was first converted into the hydroxide form ([EMIM][OH]) using an anion exchange resin (Amberlite IRN-87, Purolite) in methanol (99.8%, HPLC Grade, Fisher Scientific). Before use, the Amberlite resin was washed multiple times with methanol and vacuum-dried at room temperature to remove impurities. The anion exchange reaction proceeded until no silver halide precipitation was observed in a silver nitrate test, confirming complete halide removal.

In the second step, the [EMIM][OH] was reacted with the anion precursors under continuous stirring at room temperature overnight, allowing the acid-base reaction to proceed to completion, forming the desired IL and water as a byproduct. Excess solvent and residual water were removed via rotary evaporation at 50 °C for 1 h, followed by vacuum drying at 50 °C for 24 h. While anion precursor was pyrrole-2carbonitrile (2-CNpyrH, 99%, Thermo-Fisher) For [EMIM][2-CNpyr], 1,2,4-triazolide (97%, MilliporeSigma) was used for [EMIM][124-Triz] synthesis.

Similar procedure has been followed for the synthesis of [EMMIM][2-CNpyr] with [EMMIM][Cl] (97%, Thermo Scientific Chemicals) as cation precursor.

Synthesized ILs were confirmed by ^{1}H and ^{13}C nuclear magnetic resonance (NMR) spectroscopy using a Bruker Ascend 500 MHz spectrometer in deuterated dimethyl sulfoxide (DMSO-d6, 99.9% isotopic, Thermo Scientific). All NMR measurements were performed using the same instrument and solvent for consistency. Quantitative ^{13}C NMR samples were prepared using 0.1M chromium(III) acetylacetonate (99%, Sigma-Aldrich) in DMSO-d6, with NMR tubes purchased from Bruker. NMR confirmations of synthesis are given in Figs. S1–S3 in supplementary material.

Transient voltammetry.—Linear sweep voltammetry (LSV) experiments were performed using a three-electrode configuration in a single-compartment electrochemical cell at a scan rate of 10 mV s^{-1}, utilizing a VSP-300 electrochemical workstation (Bio-Logic). A silver (Ag) microelectrode (12 μm dia., BaSi Research Products) served as the working electrode, while a 4 cm^2 nickel mesh (99.9%, CAULYS) functioned as the counter electrode, both immersed in a 6 ml electrolyte solution. The Ag/Ag^+ reference electrode was prepared by immersing an Ag wire in a 10 mM silver nitrate ($AgNO_3$) solution containing 0.1 M tetraethylammonium perchlorate (TEAP, >98%, BeanTown Chemical) in acetonitrile (99.9%, Sigma-Aldrich).

Square wave voltammetry (SWV) was conducted using the same three-electrode setup, applying a 5 mV pulse height, −10 mV step height, and 50 ms pulse width. Before each experiment, the Ag microelectrode was mechanically polished with a 0.3 μm alumina suspension, followed by rinsing and sonication in deionized water, then acetonitrile, to ensure a clean and reproducible surface.

The base electrolyte solution for voltammetry experiments was prepared by dissolving 0.1 M tetraethylammonium tetrafluoroborate ([TEA][BF_4], 99%, Sigma Aldrich) in acetonitrile. 20 mM of 1,3,-dimethyl-2-carboxylate-imidazolium ([$MMIM^+$–COO^-], 80%, Sigma-Aldrich), pyrrole-2-carbonitrile (2-CNpyrH), 1-ethyl-3-methylimidazolium tetrafluoroborate ([EMIM][BF_4]), [EMIM][2-CNpyr]), [EMMIM][2-CNpyr], and [EMIM][124-Triz] were then added to the base electrolyte for RCC measurements. The concentration was determined based on the solubility limit of [$MMIM^+$–COO^-] in acetonitrile.

To distinguish chemisorbed CO_2 species from physisorbed CO_2, neat ILs were first saturated with CO_2 (99.995%, Airgas), then diluted in the base electrolyte, and maintained under a N_2 atmosphere (99.999%, Airgas) at 5 sccm flow rate throughout the experiments, unless otherwise specified, to eliminate any physisorbed CO_2 in the electrolyte.

Constant potential electrolysis (CPE) and product analysis.—The CPE experiments were carried out at −2.1 V vs Ag/Ag^+ for a duration of 1 h in a two-compartment H-cell setup, with the anolyte comprising 0.5 M [EMIM][2-CNpyr] in acetonitrile. Throughout the CPE duration, N_2 (10 sccm) was continuously passed into the

electrolyte reservoir for pre-CO_2 saturated electrolysis experiments. Gas chromatography (Agilent 990 MicroGC, Agilent Technologies) equipped with two thermal conductivity detectors (TCD) was directly connected to the headspace of the catholyte chamber reservoir for the analysis of gaseous electrolysis products. The details of the gas analysis procedure is further detailed in SI. Liquid samples were analyzed by ^{1}H and ^{13}C nuclear magnetic resonance (NMR) using a Bruker Ascent 500 MHz spectrometer in DMSO-d6.

Before each experiment, the water content in the electrolyte was measured using Karl-Fischer titration (Metrohm, 899 Coulometer) and confirmed to be below 500 ppm for all samples.

Results and Discussion

Electrochemical behavior of chemisorbed CO_2 species.—To probe the chemisorbed CO_2 reduction specifically, LSV was performed where the bifunctional IL was first saturated with CO_2 prior to introducing to the base electrolyte (0.1 M [TEA][BF_4] in acetonitrile). The LSV was then performed under N_2; in this way the physisorbed CO_2 was minimized (referred as "pre-CO_2"). Figure 2a provides a comparison of LSVs conducted with 20 mM [EMIM][2-CNpyr] in the base electrolyte with Ag microelectrode under different atmospheric conditions. Pre-CO_2 conditions (solid) were maintained under N_2 after initially saturating the neat IL with CO_2 to isolate chemisorbed species. Fully CO_2-saturated (dotted) conditions were performed under a continuous CO_2 atmosphere, ensuring both physisorbed and chemisorbed CO_2 were present in the electrolyte. For reference, LSVs were also conducted in an electrolyte that was only exposed to N_2 (dashed), serving as a control to examine background electrochemical behavior. As shown in the LSVs recorded from open circuit potential to −3.0 V *vs* Ag/Ag^+, the dashed line (under N_2) and the dotted line (under CO_2) exhibit distinct shifts in the voltammetry curves, indicating electron transfer reactions involving different species at different potentials. Under pre-CO_2 conditions (solid line), the onset potential is at −2.1 V *vs* Ag/Ag^+, which is more negative than the onset potential under fully CO_2-saturated conditions (dotted line, −1.9 V *vs* Ag/Ag^+). This difference suggests that the reduction at −1.9 V *vs* Ag/Ag^+ corresponds to physisorbed CO_2, as previously reported,[13,15] while chemisorbed CO_2 adducts require a higher overpotential for electrochemical reduction compared to physisorbed CO_2.

To further investigate the distinct electron transfer events observed in the LSVs, where changes in the voltammetry curves suggested the reduction of different CO_2-bound species at varying potentials, SWV was performed. In Fig. 2b, the single peak observed at −2.6 V vs Ag/Ag^+ under N_2 (dashed line) corresponds to the

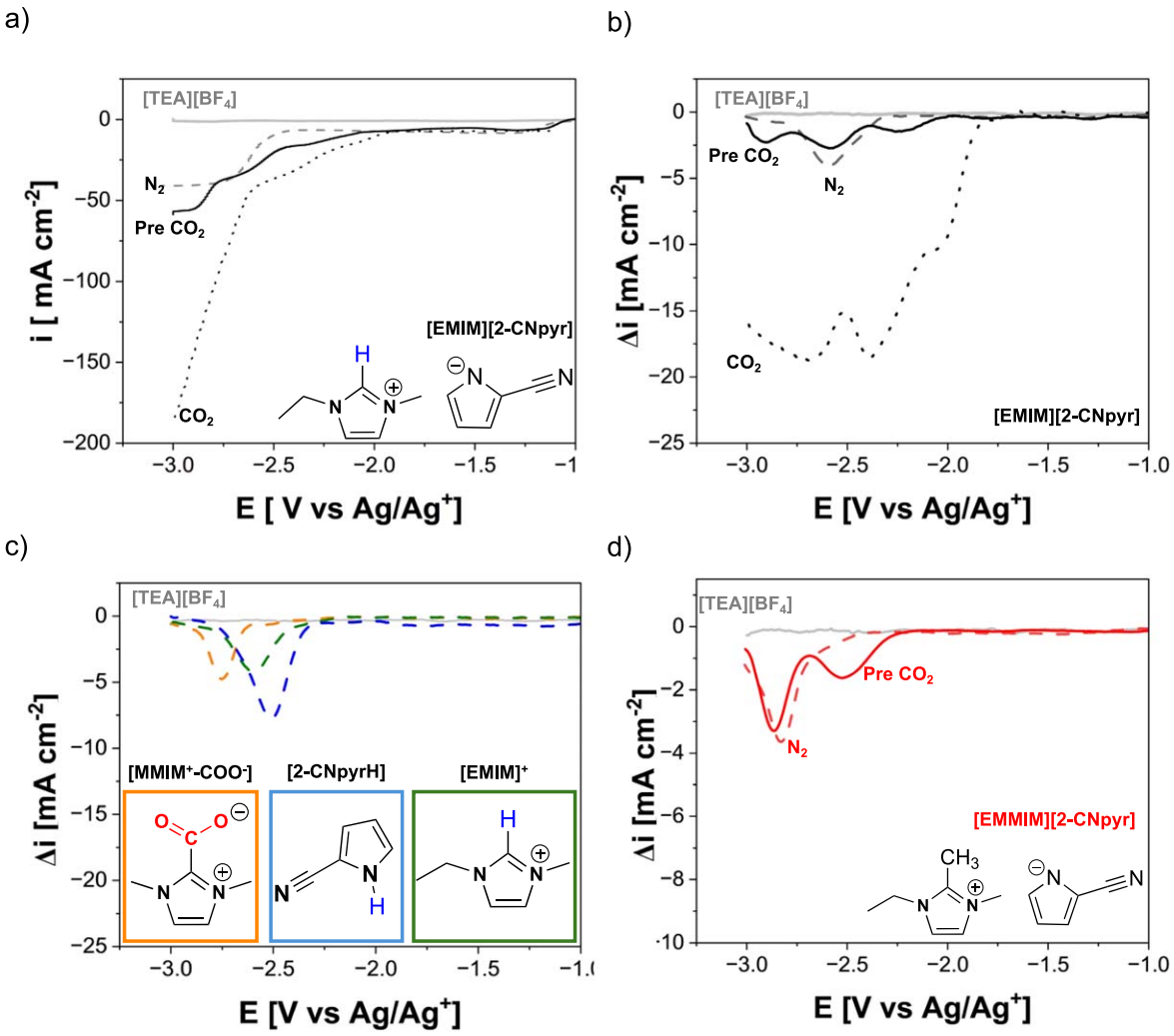

Figure 2. (a) LSVs recorded at a 10 mV s^{-1} scan rate on Ag microelectrode; comparing the base electrolyte (0.1 M [TEA][BF_4] in acetonitrile) under N_2 (solid gray line), 20 mM [EMIM][2-CNpyr] under N_2 (dashed black line), pre-CO_2-saturated electrolyte (solid black line) under N_2, and fully CO_2-saturated electrolyte (dotted black line) under CO_2 atmosphere. (b) SWVs of the same electrolytes under same conditions given in (a), (c) SWVs of individual components (20 mM) under N_2 atmosphere, representing species contributing to the microenvironment formed by [EMIM][2-CNpyr] upon CO_2 chemisorption, as depicted in Fig. 1. $[EMIM]^+$ is introduced as [EMIM][BF_4] to ensure a consistent anion with the supporting electrolyte. (d) SWVs of 20 mM [EMMIM][2-CNpyr] under N_2 (dashed red line) and pre-CO_2-saturated conditions (red solid line).

reduction of $[EMIM]^+$. In the case of pre-CO_2 conditions (solid line), where the chemisorbed CO_2 adducts shown in Fig. 1 are present in the electrolyte under N_2 atmosphere, three distinct peaks are seen at −2.1, −2.6 V, and −2.8 V vs Ag/Ag^+. Similar features are also seen in fully CO_2 saturated electrolyte (dotted line), with an additional reduction at −1.9 V vs Ag/Ag^+ corresponding to the reduction of physisorbed CO_2, consistent with the LSV curve in Fig. 2a. However, the electron transfer events corresponding to the chemisorbed species are not well resolved under fully-CO_2 saturated conditions.

To better distinguish the electrochemical behaviors of the individual chemisorbed CO_2 species, the microenvironment is reconstructed by introducing the analogous components individually in SWV measurements as presented in Fig. 2c. First, the readily available 1–3-methylimidazolium 2-carboxylate ([$MMIM^+$–COO^-], orange line in Fig. 2c) was probed as an analog for the [$EMIM^+$–COO^-] complex (carboxylate) and the peak observed at −2.7 V vs Ag/Ag^+ is attributed to the reduction of the carboxylate in [$MMIM^+$–COO^-], which exhibits the most cathodic peak among those observed in Fig. 2c. This correlation allows us to assign the most cathodic peak in Fig. 2b to the reduction of the carboxylate adduct. This result corroborates the previously discussed notion in the literature[16] that carboxylate adducts are electrochemically inactive under standard CO_2 electrolysis conditions (−2.1 V vs Ag/Ag^+ in non-aqueous IL electrolytes),[15,17] thus requiring a substantial overpotential.

The second key species introduced to the electrolyte was 2-CNpyrH (represents the protonated [2-CNpyr]$^-$). The reduction potential of 2-CNpyrH (blue line) is seen at −2.5 V vs Ag/Ag^+ in Fig. 2c. The third specie examined was $[EMIM]^+$ introduced through [EMIM][BF_4] that has the same unreactive anion as the supporting salt in the base electrolyte and the SWV peak at −2.6 V vs Ag/Ag^+ corresponds to $[EMIM]^+$ reduction (green line in Fig. 2c). Since both 2-CNpyrH and $[EMIM]^+$ reduction reactions appear at −2.5 to −2.6 V vs Ag/Ag^+ potential range when individually probed, we conclude that the SWV peak in the same region seen in Fig. 2b for pre-CO_2 [EMIM][2-CNpyr] (black solid line) encompasses the simultaneous reduction events of the cation and the protonated anion. The most anodic peak in Fig. 2b for pre-CO_2 electrolyte, observed at −2.1 V vs Ag/Ag^+, indicates the presence of a specie in the chemisorbed CO_2 environment that has not yet been experimentally replicated in Fig. 2c: the carbamate adducts ([2-CNpyr–$COO]^-$). The distinct position of this peak suggests that carbamate may play a critical role as a participant for RCC; meaning not as difficult to utilize the chemisorbed CO_2 as in the case of the carboxylate.

To prevent the carboxylate formation and allow direct CO_2 absorption exclusively toward carbamate species, 1-ethyl-2,3-methylimidazolium 2-cyanopyrollide ([EMMIM][2-CNpyr]) was used, where the C_2-position of the imidazolium ring is blocked by a methyl group. $[EMMIM]^+$, without a transferrable proton, prevents covalent CO_2 binding to the cation, hence no 2-CNpyrH formation, thus allowing isolation and examination of the anion-CO_2 adduct (i.e., carbamate) as the only chemisorbed CO_2 specie. [EMMIM][2-CNpyr] is also widely used as an ideal benchmark in the literature to study the effect of methylation on both capture[7] and conversion.[10,17,18] As shown in Fig. 2d, with pre-CO_2 [EMMIM][2-CNpyr] electrolyte (solid line), a new peak emerges at −2.5 V vs Ag/Ag^+ compared to the only N_2 exposed electrolyte (dashed line). Since the only additional species forming under pre-CO_2 conditions is the [2-CNpyr–$COO]^-$ adduct, this newly emerging peak is assigned to carbamate. The slightly more cathodic reduction of carbamate in [EMMIM][2-CNPyr] (−2.5 V) compared to [EMIM][2-CNpyr] (−2.1 V) is due to the differences in the microenvironment of the interface between the two systems. Additionally, the reduction of $[EMMIM]^+$ is observed at −2.7 V vs Ag/Ag^+, indicating that the methyl substitution at the C_2-position enhances the stability of the cation $[EMMIM]^+$ compared to $[EMIM]^+$. This highlights the strong C–C bond formation, similar to [$EMIM^+$–COO^-].

It seems counterintuitive to consider anions participating in an electrochemical reduction process, especially on a negatively polarized surface where classical electrical double layer (EDL) models predict their exclusion. Yet, the experimental observations presented in Fig. 2 consistently indicate the carbamate species are actively participating in the reduction cycle. Classical EDL models, such as the Gouy-Chapman-Stern theory, suggest that co-ions are excluded from the near-surface region due to electrostatic repulsion. These models predict a counter-ion-dominated bound ion layer and a diffuse layer with a gradually decreasing ion concentration extending into the bulk.[3] Two key parameters govern this classical framework: the Bjerrum length (l_B) and the Debye screening length (λ_D). l_B defines the distance at which the electrostatic interaction energy between two charges equals thermal energy (k_BT). In polar solvents like water (dielectric constant $\varepsilon = 80$), l_B is relatively short (~7 Å), and thermal energy dominates, weakening ionic interactions. In contrast, in less polar solvents such as acetonitrile ($\varepsilon = 36$), l_B increases to 30–40 Å, indicating stronger electrostatic interactions and the likelihood of ion pairing. λ_D measures the distance over which electrostatic interactions are screened.[19] Even though classical Debye–Hückel theory predicts shorter λ_D as the ion concentration increases, long screening lengths up to 15 nm are reported for ILs, indicating that they can form ion pairs and only a small fraction of ions contribute to the charge screening.[20] Although the electrolyte concentrations are dilute in this study (0.1 M supporting salt + 20 mM IL), electrostatic as well as hydrogen bonding interactions between cations and anions may persist in the bulk electrolyte due to low dielectric constant of acetonitrile.[21] In addition, the dielectric constant of acetonitrile further collapses at the interface due to preferred molecular orientation, allowing ion pairs at the interface.[22,23] At high applied potential used for CO_2RR -exceeding 2 V, far beyond the thermal energy scale k_BT (~25 meV at room temperature), the electrode-electrolyte interface enters a non-classical regime. Here, ion-ion correlations and clustering can dominate the EDL structure, defying classical models such as Gouy-Chapman-Stern. While we acknowledge that non-classical EDL behaviors are associated with concentrated electrolytes or neat ILs, we hypothesize that these non-classical dynamics and adsorption of pyrrole ring allow co-ions, such as the [2-CNpyr–$COO]^-$ carbamate complex, to persist in the near-surface region and actively participate in electrochemical processes.

Microenvironmental factors for RCC.— *$[EMIM]^+$ vs $[EMMIM]^+$ on electro-kinetics.*—For both [EMIM][2-CNpyr] and [EMMIM][2-CNpyr], the ability to form an anion-CO_2 complex is a shared feature; however, with the methyl block on the C_2 carbon in $[EMMIM]^+$, carboxylate formation is not possible. These ILs also differ in their electrochemical behavior; [EMIM][2-CNpyr] shows a significantly earlier onset potential for carbamate reduction (Fig. 2b) compared to [EMMIM][2-CNpyr] (Fig. 2d). Further, the driving force required to enhance reaction rate also varies between the two reactive ILs. Figure 3a presents Tafel plots for [EMIM][2-CNpyr] and [EMMIM][2-CNpyr], revealing Tafel slopes of 203 mV dec^{-1} and 263 mV dec^{-1}, respectively. Assuming the rate-determining step is the first electron transfer to the anion-CO_2 complex, the calculated α values are 0.29 and 0.22 for [EMIM][2-CNpyr] and [EMMIM][2-CNpyr], respectively. These values can be attributed to the anionic nature of the electroactive species getting reduced, causing deviation of α from ideal values, and further emphasizing the importance of the microenvironment. These values suggest sluggish reaction kinetics with possible deviation of charge transfer coefficient (α) from 0.5; consistent with prior literature of anionic electroreduction reactions.[24]

Electrostatic stabilization and hydrogen bonding.—To further understand the impact of the microenvironment on the differences in

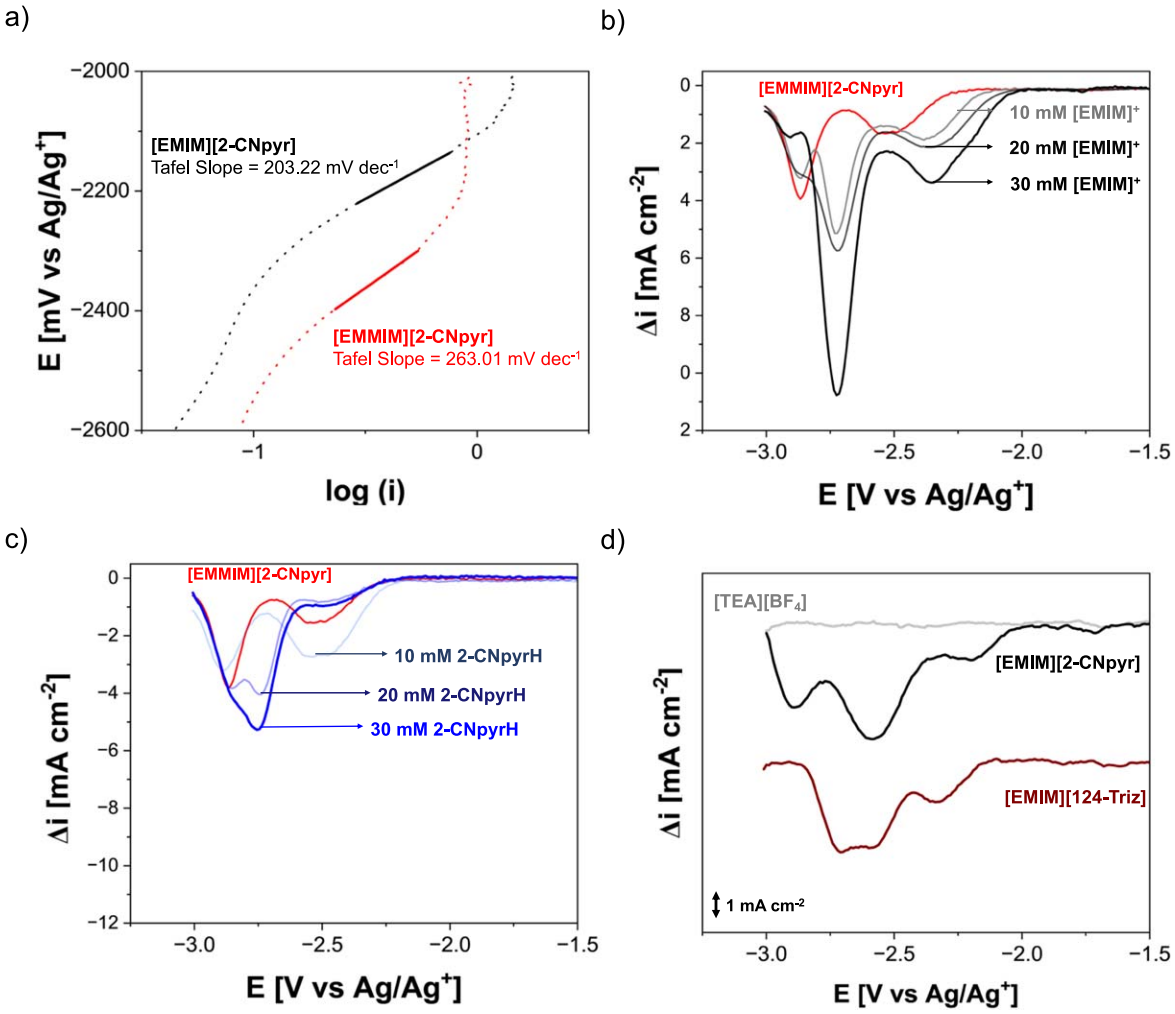

Figure 3. (a) Tafel plots for [EMIM][2-CNpyr] and [EMMIM][2-CNpyr], illustrating the impact of microenvironment ($R^2 = 0.999$ for both). The base unit of current density used is mA cm^{-2}. (b) SWV curves showing the anodic shift in $[2\text{-CNpyr–COO}]^-$ reduction onset potential as $[EMIM]^+$ is incrementally added to 20 mM [EMMIM][2-CNpyr], replacing $[EMMIM]^+$ at the interface. (c) SWV curves demonstrating replacement of $[2\text{-CNpyr–COO}]^-$ by neutral 2-CNpyrH at increasing 2-CNpyrH concentrations, added to a 20 mM [EMMIM][2-CNpyr] base electrolyte, (d) SWV comparison of [EMIM][2-CNpyr] and [EMIM][124-Triz], highlighting the impact of anion basicity. All electrolytes were prepared in acetonitrile with 0.1 M $[TEA][BF_4]$ as the supporting salt. Tafel plot scan rate = 10 mV s^{-1}. Pulse height = 5 mV, step height = −10 mV, pulse width = 50 ms.

electrochemical behavior of [EMIM][2-CNpyr] and [EMMIM][2-CNpyr], specific attention was given to the roles of the cation and the protonated anion (2-CNpyrH). These components were chosen due to their distinctive potential to modulate the electrostatic stabilization of the anion-CO_2 complex and their hydrogen-bonding capacity, both of which are critical to facilitating RCC. Figure 3b presents the SWV results where $[EMIM]^+$ was introduced at varying concentrations (10, 20 and 30 mM) in the form of [EMIM][2-CNpyr] into a pre-CO_2 [EMMIM][2-CNpyr] electrolyte (20 mM). As the concentration of $[EMIM]^+$ increases, it progressively replaces $[EMMIM]^+$ at the electrode surface, as evidenced by the increase in the $[EMIM]^+$ reduction peak and the corresponding decrease in the $[EMMIM]^+$ peak. Concurrently, the onset potential of the $[2\text{-CNpyr–COO}]^-$ reduction also shifts anodically, underscoring the superior ability of $[EMIM]^+$ to stabilize the anion complex at the interface compared to $[EMMIM]^+$.

The role of the protonated anion, 2-CNpyrH, was similarly explored by adding it at concentrations of 10, 20, and 30 mM to a 20 mM pre-CO_2 [EMMIM][2-CNpyr] electrolyte, as shown in Fig. 3c. At 10 mM, the reduction peak for the $[2\text{-CNpyr–COO}]^-$ complex broadens and enhances. However, at higher 2-CNpyrH concentrations, a distinct new peak emerges while the $[2\text{-CNpyr–COO}]^-$ peak diminishes. This behavior suggests that the initial increase in current may be due to overlapping of 2-CNpyrH reduction peak with $[2\text{-CNpyr–COO}]^-$ and that higher 2-CNpyrH levels lead to replacement of $[2\text{-CNpyr–COO}]^-$ at the interface. As a result, accessibility of the carbamate species to the electrode surface is reduced with increased 2-CNpyrH. Notably, the $[EMMIM]^+$ reduction peak remains largely unchanged, confirming that the observed effects are primarily driven by the interplay between 2-CNpyrH and the anion-CO_2 complex. These findings emphasize that the interfacial compositional variations strongly influence electrochemical response and reflect the highly dynamic nature of reactive IL microenvironments in RCC.

The relatively smaller $[EMIM]^+$ can form a denser and more ordered EDL compared to the bulkier $[EMMIM]^+$.[13,18,25] This compact packing is shown to enhance electrostatic stabilization, and here the stabilization of the anion-CO_2 complex can be attributed to this feature, likely cation forming an ion pair with anion-CO_2 complex that facilitate electron transfer at lower potentials. Even though the introduction of 2-CNpyrH alters the microenvironment by introducing hydrogen-bonding interactions, which have been previously shown to shift the onset potential of physisorbed CO_2 reduction,[11] it appears to impede the proximity of the $[2\text{-CNpyr–COO}]^-$ complex to the electrode, reducing its availability for RCC, as demonstrated in Fig. 3c. These findings underscore the

sensitivity of the microenvironment on the cation structure and hydrogen-bond donors.

Anion basicity.—Figure 3d examines the influence of anion basicity by comparing [EMIM][2-CNpyr], which contains highly basic anion (pK_a = 15),[10] with [EMIM][124-Triz], which has a moderately basic anion (pK_a = 10.04).[26] Both ILs exhibit three distinct peaks in their pre-CO_2 SWV curves, suggesting similarities in electrochemical behavior of chemisorption species. Despite the similarity, the onset potential for anion–CO_2 complex in [EMIM][124-Triz] is shifted to a more cathodic potential compared to [EMIM][2-CNpyr]. Surprisingly, the carboxylate species in [EMIM][124-Triz] shows an onset potential that is more positive than its counterpart in [EMIM][2-CNpyr]. The middle peak in both cases correspond to the overlapping reduction of the cation and the protonated anion (see Fig. S4 for component analysis of [EMIM][124-Triz]).

Electrolysis of chemisorbed CO_2.—To understand the products from the probed electron transfer reactions, particularly the RCC products with the acetonitrile electrolyte containing the bifunctional IL on Ag (1 cm^2 area), electrolysis experiments in an H-cell was performed under N_2 atmosphere. The headspace of the catholyte chamber was monitored by gas chromatography to identify the gaseous products. Figure 4a displays the chronoamperometry results and the corresponding faradaic efficiencies (FE) during a 1 h electrolysis at −2.1 V (red) and −2.3 V (blue) vs Ag/Ag^+. The stable current observed over time underscores sustained electrochemical activity. While the average FE of 95% for CO production at −2.1 V vs Ag/Ag^+ demonstrates the high selectivity of RCC, stepping the potential up to −2.3 V vs Ag/Ag^+ results in a decrease in CO FE from 95% to 80%, with HER activity increasing the production of H_2 to 20% on average over the course of the 1 h electrolysis.

The electrolyte itself was also examined by NMR for any liquidus products and other compositional changes. While no liquidous RCC products were detected after electrolysis such as formate, a compositional variation of the carbamate and carboxylate compounds were noted in quantitative ^{13}C NMR (Fig. S5; see also ^1H NMR in Fig. S6). Figure 4b shows the measured concentrations of carbamate and carboxylate in the pre-CO_2-saturated electrolyte immediately before electrolysis (green) and after electrolysis at −2.1 V vs Ag/Ag^+ (red) and −2.3 V *vs* Ag/Ag^+ (blue).The results reveal a significant decrease in carbamate composition during electrolysis after 1 h. Interestingly, carboxylate composition also decreases even though it is not electrochemically active at the electrolysis conditions. The decrease in carboxylate composition is attributed to a shift in the speciation equilibrium as a result of the diminished CO_2 partial pressure over the electrolyte, consistent with the prior CO_2 absorption product analysis of this IL.[27]

Combining key findings from voltammetry measurements, electrolysis product analysis, and the captured interfacial speciation trends, a physical model of the interface emerges as illustrated in Fig. 4c. The interaction between $[EMIM]^+$ and carbamate at the electrode surface suggests that they co-adsorb on the electrode surface. The electron transfer to carbamate species is initiates a reaction in which the $–COO^-$ moiety detaches from the carbamate, leading to the subsequent replacement of the anion at the interface by protonated anion (2-CNpyrH) to preserve charge neutrality at the interface. Further, the formation of H_2 at the increased potentials indicates the presence and participation of protonated anions in the reaction pathway. Despite the overlapping reduction potentials for protonated anion (2-CNpyrH) and $[EMIM]^+$, the increase in $[EMIM]^+$ concentration as probed by NMR after electrolysis (Fig.

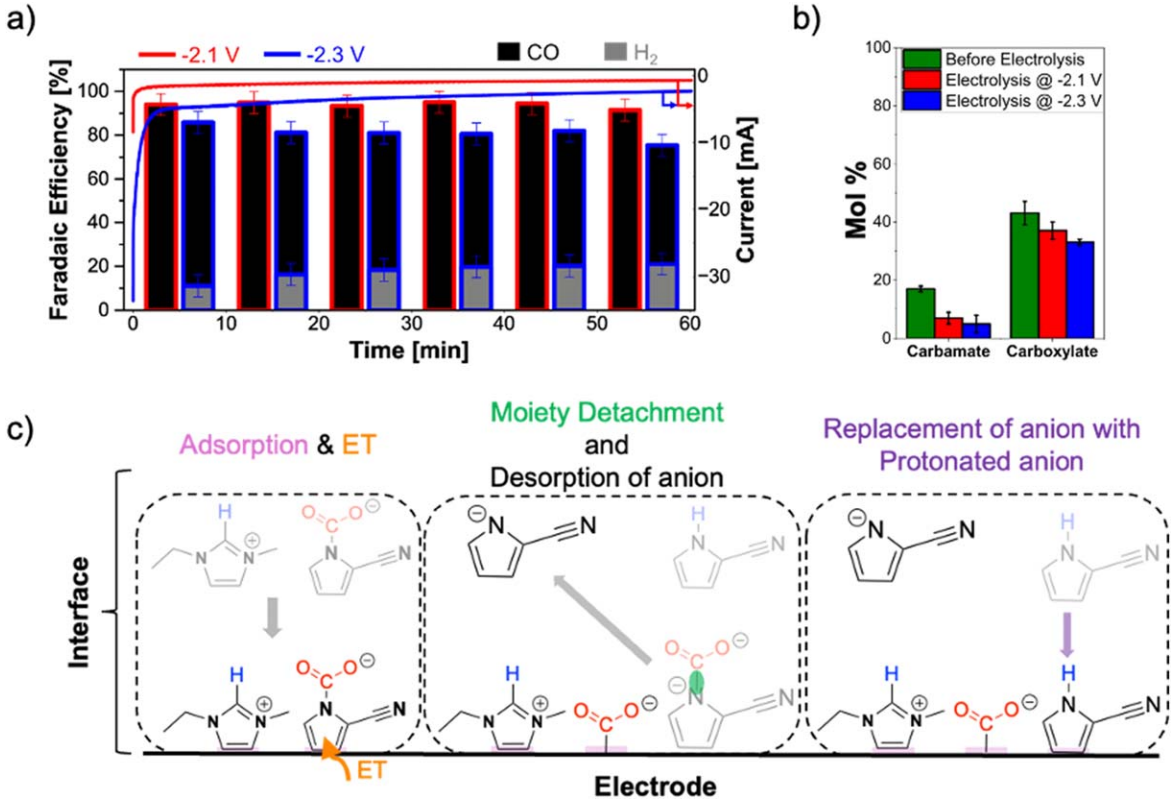

Figure 4. (a) Chronoamperometry curves of pre-CO_2-saturated reactive IL at −2.1 V and −2.3 V *vs* Ag/Ag^+ during a 1 h electrolysis, along with faradaic efficiencies for CO and H_2 production. The [EMIM][2-CNpyr] concentration was maintained at 0.5 M in 0.1 M [TEA][BF_4] containing acetonitrile. (b) Bar plot illustrating the changes in CO_2 chemisorption species post-electrolysis compared to a non-electrolyzed sample, highlighting variations in carbamate and carboxylate levels. (c) Schematic representation of interfacial phenomena during RCC, depicting the interactions between electrochemically active species and the cation. While the $[EMIM]^+$ and CO_2 are shown in close spatial proximity, this is intended to represent possible electrostatic interactions and stabilization of the CO_2 radical anion by the cation. The carboxylate adduct is omitted for clarity, focusing on species directly participating in the electrochemical activity.

S6) reinforces the idea that protonated anions, rather than $[EMIM]^+$, are responsible for the increased H_2 at higher potentials.

Conclusions

This study highlights the dynamic and complex nature of the microenvironment formed by reactive ILs in governing the electrochemical behavior and electrocatalytic activity of chemisorbed CO_2 species. The findings specific to the bifunctional IL, [EMIM][2-CNpyr], reveal that the microenvironment is able to sustain the anion–CO_2 carbamate complex at negatively polarized surfaces. A key insight from this study is the critical role of the anion–CO_2 carbamate complex in facilitating RCC at lower overpotentials compared to other chemisorbed species such as cation–CO_2 carboxylate complex. While the majority of the chemisorbed CO_2 exists as cation–CO_2 complexes, these species require significantly higher overpotentials for utilization in RCC. The observed differences in reduction behavior of chemisorbed species point to underlying variations in structural and electronic factors. This underscores the need to further explore the dynamic interplay between the components of the interface via computational methods. While making use of ILs that promote the anion dominated CO_2 formation is feasible, strategies to activate carboxylates is needed to enhance their electrochemical utilization in RCC.

Acknowledgments

This research was supported by NSF CAREER award (no. 2045111) from the Division of Chemical, Bioengineering, Environmental and Transport Systems (CBET), Interfacial Engineering, and Electrochemical Systems for electrochemical measurements, which supported O.K.C's contributions. S.D. was supported by the Center for Closing the Carbon Cycle (4 C) EFRC, under award # DE-SC0023427, for electrolysis product analysis. The authors also acknowledge the NMR Instrumentation Facility at the Department of Chemistry, Case Western Reserve University, for providing access to analytical instrumentation.

ORCID

Oguz Kagan Coskun https://orcid.org/0000-0002-8452-8552
Saudagar Dongare https://orcid.org/0000-0001-6782-0028
Burcu E. Gurkan https://orcid.org/0000-0003-4886-3350

References

1. J. Chen, Y. Xu, P. Liao, H. Wang, and H. Zhou, "Recent progress in integrated CO_2 capture and conversion process using dual function materials: a state-of-the-art review." *Carbon Capture Science & Technology*, **4**, 100052 (2022).
2. A. M. Appel and J. Y. Yang, "Maximum and comparative efficiency calculations for integrated capture and electrochemical conversion of CO_2." *ACS Energy Lett.*, **9**, 768 (2024).
3. O. K. Coskun, M. Muñoz, S. Dongare, W. Dean, and B. E. Gurkan, "Understanding the electrode–electrolyte interfaces of ionic liquids and deep eutectic solvents." *Langmuir*, **40**, 3283 (2024).
4. S. Dongare, M. Zeeshan, A. S. Aydogdu, R. Dikki, S. F. Kurtoğlu-Öztulum, O. K. Coskun, M. Muñoz, A. Banerjee, M. Gautam, and R. D. Ross, "Reactive capture and electrochemical conversion of CO_2 with ionic liquids and deep eutectic solvents." *Chem. Soc. Rev.*, **53**, 8563 (2024).
5. S. Oh, O. Morales-Collazo, and J. F. Brennecke, "Cation–Anion interactions in 1-Ethyl-3-methylimidazolium-based ionic liquids with aprotic heterocyclic anions (AHAs)." *J. Phys. Chem. B*, **123**, 8274 (2019).
6. B. Gurkan et al., "Molecular design of high capacity, low viscosity, chemically tunable ionic liquids for CO_2 capture." *The Journal of Physical Chemistry Letters*, **1**, 3494 (2010).
7. Y.-Y. Lee, D. Penley, A. Klemm, W. Dean, and B. Gurkan, "Deep eutectic solvent formed by imidazolium cyanopyrrolide and ethylene glycol for reactive CO_2 separations." *ACS Sustainable Chemistry & Engineering*, **9**, 1090 (2021).
8. N. Hollingsworth, S. R. Taylor, M. T. Galante, J. Jacquemin, C. Longo, K. B. Holt, N. H. De Leeuw, and C. Hardacre, "Reduction of carbon dioxide to formate at low overpotential using a superbase ionic liquid." *Angew. Chem. Int. Ed.*, **54**, 14164 (2015).
9. Z.-Z. Yang, Y.-N. Zhao, and L.-N. He, "CO2 chemistry: task-specific ionic liquids for CO_2 capture/activation and subsequent conversion." *RSC Adv.*, **1**, 545 (2011).
10. S. Dongare, O. K. Coskun, E. Cagli, K. Y. C. Lee, G. Rao, R. D. Britt, L. A. Berben, and B. Gurkan, "A bifunctional ionic liquid for capture and electrochemical conversion of CO_2 to CO over silver." *ACS Catal.*, **13**, 7812 (2023).
11. O. K. Coskun, S. Dongare, B. Doherty, A. Klemm, M. Tuckerman, and B. Gurkan, "Tailoring electrochemical CO_2 reduction on copper by reactive ionic liquid and native hydrogen bond donors." *Angew. Chem.*, **136**, e202312163 (2024).
12. S. Dongare, O. K. Coskun, E. Cagli, J. S. Stanley, A. Q. Mir, R. S. Brower, J. M. Velázquez, J. Y. Yang, R. L. Sacci, and B. Gurkan, "Key experimental considerations when evaluating functional ionic liquids for combined capture and electrochemical conversion of CO_2." *Langmuir*, **40**, 9426 (2024).
13. O. K. Coskun, Z. Bagbudar, V. Khokhar, S. Dongare, R. E. Warburton, and B. Gurkan, "Synergistic effects of the electric field induced by imidazolium rotation and hydrogen bonding in electrocatalysis of CO_2." *JACS*, **146**, 23775 (2024).
14. Y.-Y. Lee, K. Edgehouse, A. Klemm, H. Mao, E. Pentzer, and B. Gurkan, "Capsules of reactive ionic liquids for selective capture of carbon dioxide at low concentrations." *ACS Appl. Mater. Interfaces*, **12**, 19184 (2020).
15. B. Liu, W. Guo, and M. A. Gebbie, "Tuning ionic screening to accelerate electrochemical CO_2 reduction in ionic liquid electrolytes." *ACS Catal.*, **12**, 9706 (2022).
16. L. Sun, G. K. Ramesha, P. V. Kamat, and J. F. Brennecke, "Switching the reaction course of electrochemical CO_2 reduction with ionic liquids." *Langmuir*, **30**, 6302 (2014).
17. W. Guo, B. Liu, and M. A. Gebbie, "Suppressing Co-Ion generation via cationic proton donors to amplify driving forces for electrochemical CO_2 reduction." *The Journal of Physical Chemistry C*, **127**, 14243 (2023).
18. W. Guo, B. Liu, S. R. Anderson, S. G. Johnstone, and M. A. Gebbie, "Deciphering the role of aromatic cations in electrochemical CO_2 reduction: interfacial ion assembly governs reaction pathways." *J. Mater. Chem. A*, **12**, 17169 (2024).
19. M. A. Gebbie, B. Liu, W. Guo, S. R. Anderson, and S. G. Johnstone, "Linking electric double layer formation to electrocatalytic activity." *ACS Catal.*, **13**, 16222 (2023).
20. M. A. Gebbie, A. M. Smith, H. A. Dobbs, G. G. Warr, X. Banquy, M. Valtiner, M. W. Rutland, J. N. Israelachvili, S. Perkin, and R. Atkin, "Long range electrostatic forces in ionic liquids." *Chem. Commun.*, **53**, 1214 (2017).
21. H. K. Stassen, R. Ludwig, A. Wulf, and J. Dupont, "Imidazolium salt ion pairs in solution." *Chem.–Eur. J.*, **21**, 8324 (2015).
22. R. Sundararaman and K. Schwarz, "Solvent effects determine the sign of the charges of maximum entropy and capacitance at silver electrodes." *J. Chem. Phys.*, **158**, 121102 (2023), (acccessed 5/19/2025).
23. F. Ding, Z. Hu, Q. Zhong, K. Manfred, R. R. Gattass, M. R. Brindza, J. T. Fourkas, R. A. Walker, and J. D. Weeks, "Interfacial organization of acetonitrile: simulation and experiment." *The Journal of Physical Chemistry C*, **114**, 17651 (2010).
24. A. Frumkin, N. Nikolaeva-Fedorovich, N. Berezina, and K. E. Keis, "The electroreduction of the S2O82− anion." *J. Electroanal. Chem. Interfacial Electrochem.*, **58**, 189 (1975).
25. S. Noh, Y. J. Cho, G. Zhang, and M. Schreier, "Insight into the role of entropy in promoting electrochemical CO_2 reduction by imidazolium cations." *JACS*, **145**, 27657 (2023).
26. S. Couto Rodrigues, R. Silva Moratório de Moraes, G. Tavares de Almeida Pinto, M. T. Miranda Martins, P. Antunes do Nascimento, D. L. Alves Soares, A. B. Mestre Botelho, C. Cardoso Cruz, and A. C. Cunha, "A review on chemistry and methods of synthesis of 1,2,4-triazole derivatives." *The Chemical Record*, **25**, e202400190 (2025).
27. Y.-Y. Lee and B. Gurkan, "Graphene oxide reinforced facilitated transport membrane with poly (ionic liquid) and ionic liquid carriers for CO2/N2 separation." *J. Membr. Sci.*, **638**, 119652 (2021).